LETTER

Nature of the charge carriers in $LaAlO_3$-$SrTiO_3$ oxide heterostructures probed using hard X-ray photoelectron spectroscopy

A Letters Journal Exploring the Frontiers of Physics

August 2018

EPL, **123** (2018) 47003
doi: 10.1209/0295-5075/123/47003

www.epljournal.org

Nature of the charge carriers in $LaAlO_3$-$SrTiO_3$ oxide heterostructures probed using hard X-ray photoelectron spectroscopy

Sumanta Mukherjee[1], Banabir Pal[1], Indranil Sarkar[2], Ambroise van Roekeghem[3,4], Wolfgang Drube[2], H. Takagi[5,6], Jobu Matsuno[7], Silke Biermann[8] and D. D. Sarma[1(a)]

[1] *Solid State and Structural Chemistry Unit, Indian Institute of Science - Bengaluru 560012, India*
[2] *Deutsches Elektronen-Synchrotron DESY - Notkestrasse 85, D-22607 Hamburg, Germany*
[3] *Université Grenoble Alpes - F-38000 Grenoble, France*
[4] *CEA, LITEN - 17 rue des Martyrs, F-38054 Grenoble, France*
[5] *Department of Physics, University of Tokyo - Tokyo 113-0033, Japan*
[6] *Max-Plank-Institute for Solid State Research - Stuttgart D-70569, Germany*
[7] *RIKEN Center for Emergent Matter Science (CEMS) - Saitama 351-0198, Japan*
[8] *Centre de Physique Theorique, Ecole Polytechnique, CNRS UMR 7644 - F-91128 Palaiseau, France*

received on 24 August 2018; accepted by P. S. Cornaglia on 28 August 2018
published online 17 September 2018

PACS 73.20.-r – Electron states at surfaces and interfaces
PACS 79.60.Jv – Interfaces; heterostructures; nanostructures
PACS 79.60.-i – Photoemission and photoelectron spectra

Abstract – A proper investigation of the valence band electronic structure is the essential first step towards understanding the intriguing co-existence of several exotic electronic phases like ferromagnetism and superconductivity, in $LaAlO_3$-$SrTiO_3$ heterostructures. In order to comprehend the electronic structure across the $LaAlO_3$-$SrTiO_3$ oxide interface, a detailed valence band investigation has been carried out using variable energy hard X-ray photoelectron spectroscopy and signatures of both low-energy coherent and high-energy features have been observed in the valence band spectra. Our combined experimental and theoretical study suggests that the charge carriers at the interface are weakly correlated and the high-energy feature does not arise from the lower Hubbard band. Instead, this high-energy feature is attributed to in-gap states induced by oxygen vacancies and possible polaron formation.

Introduction. – The intriguing appearance of a two-dimensional electron gas (2DEG) [1,2] coupled with superconductivity [3–6] and ferromagnetism [5–7] in heterostructures of two band-insulators, namely $LaAlO_3$ (LAO) and $SrTiO_3$ (STO) has triggered huge enthusiasm in the field of condensed-matter science in the last decade. There is a general agreement, supported by experimental evidence, that these interesting properties arise from electron doping of the Ti 3*d* states in $SrTiO_3$ [8–14]. However there is a substantial controversy concerning the origin of the mechanism of doping of Ti 3*d* levels, with suggestions of a growing polar field within LAO [1,15], various electronic [1,15] and atomic [16] reconstructions, and oxygen vacancies [8,17–21] having been proposed as responsible. Irrespective of the exact origin of the doping of electrons responsible for these unusual properties, the fact that 3*d* electrons, archetypes of strong correlation physics, are involved makes it necessary to understand the role of Coulomb correlation within this 2DEG in order to understand the electronic structure responsible for appearances of such exotic phases. This aspect can be most directly probed by photoemission spectroscopy that can map out the single-electron ionization spectrum for any system including electron-doped $SrTiO_3$ [22–24] and it is well known that the low-energy part of such spectra carry important information concerning correlation effects [22–24] as well as oxygen vacancy induced states [25–28]. However, there are limitations in applying photoemission techniques to address this question in LAO-STO heterostructures. In the low carrier concentration limit, states close to the

(a)E-mail: sarma@sscu.iisc.ernet.in

Fermi energy, and, therefore, directly responsible for these physical properties, are far below the limit of detection in normal photoemission techniques. Even in samples with higher carrier concentrations, the overlayer coverage of 2–3 nm of LAO makes it challenging to obtain a good-quality spectrum [29] of these low-energy valence band states. There are few reports [10–12,30–32] of the valence band structure from LAO-STO heterostructures, but in all of these cases, the technique of resonant photoemission was employed to enhance spectral features of the Ti 3*d* manifold, making valence band features more easily visible. This is achieved in resonant photoemission as it invokes second-order dipole matrix transition elements involving core level absorption and decay channels. However, this second-order process couples different scattering channels differently, which leads to enhancement or suppression of spectral intensity in the region near Fermi level that is or not in resonant condition. Furthermore, a theoretical understanding of such experimental information within the single-particle excitation spectra including correlation effects is difficult. On the other hand, normal hard X-ray photoemission spectroscopy (HAXPES) yielding high-kinetic-energy photoelectrons is in better agreement to the sudden approximation criterion. Under the sudden approximation the photoelectron wave function is assumed to decouple from the rest of the interacting many-electron wave function left behind. This should allow a better description of the experimental data using established theoretical methods in the sudden approximation regime of calculating many electron correlation effects in photoemission. Given the advantages of normal HAXPES [8,9,33–37], it is desirable to investigate the strong correlation effects in the low-energy states, away from any resonant process, using hard X-ray photon energies. In this article, we present such results using high photon energies to carry out photoemission valence band studies, with the high photon energy allowing us to look deep into the heterostructure.

For variable energy HAXPES measurements, we have chosen two different LAO-STO samples that were already investigated to understand the spatial distribution of the charge carrier densities and their origin using detailed core level spectroscopic measurements, as reported in ref. [8]. Core level photoemission spectroscopy helped to establish [8] that these samples have two distinctly different distributions of doped Ti 3*d* electrons, one being tied to the interface with a narrow thickness of ~ 1 nm and with an electron density of ~ 2–$5 * 10^{14}\,\mathrm{cm}^{-2}$. These carriers, being separated from the oxygen vacancies, possibly relates with the 2DEG observed in the LAO-STO system and are thus named as 2DEG in this letter. The remaining part of the doped 3*d* electron density was shown in ref. [8] to be more like a bulk doping of the STO substrate by oxygen vacancies with a charge carrier density of $\sim 6 * 10^{20}\,\mathrm{cm}^{-3}$, corresponding to a lightly doped limit with electron density per unit cell (0.03–0.06 e/uc) much lower than what is observed for the 2DEG, namely ~ 0.5 e/uc. In this sense, the average number based on Hall measurements is misleading as it integrates the bulk doping and projects it as a two-dimensional quantity leading to a value of $\sim 10^{17}\,\mathrm{cm}^{-2}$ in our samples. Here we focus only on electronic states close to the Fermi energy and related directly to the electronic structure of the doped carriers. It should be noted that these states have not been reported so far in the literature with non-resonant photoemission experiments owing to their extremely low intensity.

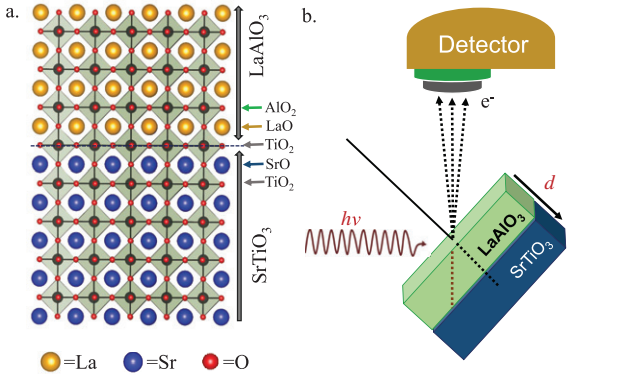

Fig. 1: (Color online) (a) A schematic representation of a TiO_2 terminated (n-type) LAO-STO heterostructure. 4 unit cells (uc) and 6 uc of LAO were grown on a TiO_2-terminated STO substrate. (b) Schematic representation of the X-ray photoelectron spectroscopy geometry.

Experimental section. – Pulsed-laser deposition was used to grow hetrostructures of LAO-STO with n-type interfaces. The samples were grown at a oxygen pressure ($pO_2 \sim 3 \times 10^{-7}$ Torr), with a laser fluence of $\sim 2\,\mathrm{Jcm}^{-2}$. Two different LAO thicknesses, namely 4 and 6 unit cells (uc) and termed in this paper 4-uc and 6-uc samples, respectively, were grown for the specific photoemission study. A representative schematics of the superlattice is shown in fig. 1(a). Resistivity measurements on both 4-uc and 6-uc samples confirm the expected metallic nature. Room temperature HAXPES measurements were performed at the HAXPES end station P09 of the Petra-III beamline, DESY, Hamburg, Germany, at a base pressure in the range of ~ 1–$2 * 10^{-9}$ mbar. Different photon energies between 3500 and 5400 eV were used for acquiring the photoelectron spectra. The overall resolution of the measurements were 500 meV and 710 meV at photon energies of 3500 eV and 5400 eV, respectively. The typical HAXPES measurement geometry is shown in fig. 1(b). In a typical measurement, the sample was mounted on a sample holder, which was connected to the ground. Additionally, a connection was made between the top LAO layer to the ground to avoid charging effect during photoemission measurements. The Fermi energy of a gold sample and the binding energy (BE) of the Au 4*f* core level spectra were used to calibrate the photon energies. A more detailed description of the sample synthesis conditions, cross-sectional transmission electron micrograph

and sheet resistance data are given in an earlier publication [8].

Results and discussion. – Figure 2(a) shows valence band spectra of the 4-uc LAO-STO system acquired with excitation energies of 3500 eV and 5400 eV. The prominent feature between 3 eV and 12 eV binding energies arises from O, Ti and Sr derived states. The visible change in the spectra between 3 and 12 eV BE at different photon energies is due to the change in the depth sensitivity and cross-sections [38]. On the other hand, very low intensity, the almost indiscernible spectral feature in fig. 2(a), appearing between 2.5 eV BE and the Fermi energy, is mainly due to Ti 3*d* like states. The nature of these low-energy occupied Ti 3*d* states is important as these electrons are responsible for the electronic properties of these heterostructures. For clarity, we show in fig. 2(b) the valence band spectra close to the Fermi energy measured at 3500 eV and 5400 eV photon energies on an expanded scale. The valence band spectra as shown in fig. 2(b) contain two features: one with a peak at ~ 0.4 eV BE, arising mainly from delocalized electrons with a finite intensity at the Fermi level and is commonly known as the coherent feature, and a second feature at around 1.2 eV BE, marked as high-energy feature. While fig. 2(b) clearly shows both coherent and high-energy spectral features, marked by arrows, the spectral intensities, particularly that of the high-energy feature is enhanced by the overlapping decaying tail of high-intensity spectral features centered around 6–8 eV BE. We have removed this spectral contribution from the decaying tail of high-energy features in the low-energy region of the Ti 3*d* spectral features by using a smooth polynomial curve between -1 eV and 2.5 eV BE. The extracted spectral features corresponding to contributions only from coherent and high-energy features are plotted in fig. 2(c). Both these plots show the coherent and high-energy features clearly. In order to ascertain that the above result is not specific to the sample investigated, we studied another sample with 6-uc LAO overlayer on STO. Following the same approach as the one adopted for the 4-uc sample, the O 2*p* contribution was subtracted from the obtained valence band spectra of the 6-uc sample and the resulting low-energy spectral features are shown in fig. 2(d). With a 50% increase of the LAO overlayer thickness of this 6-uc sample compared to the 4-uc LAO sample, the already difficult task of obtaining a spectrum of the low-energy features with a reasonable signal-to-noise ratio is rendered much harder in the 6-uc sample due to the exponential decay of the spectral intensity with the overlayer thickness. This difficulty is evident in the lower signal-to-noise ratio of the valence band spectra of the 6-uc sample recorded with three different photon energies, shown in fig. 2(d). In spite of the lower signal-to-noise ratio, the spectra in this 6-uc sample also exhibit signatures of what have been termed as coherent and high-energy features in fig. 2(b) for the 4-uc sample. It is interesting to note that these spectral features including the peak positions are consistent

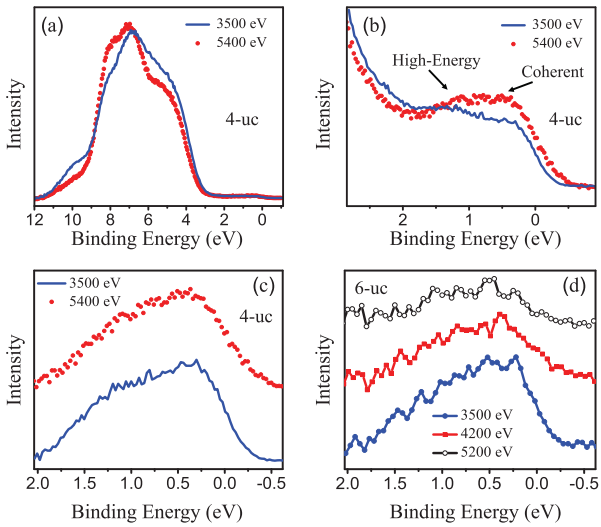

Fig. 2: (Color online) (a) Valence band spectra recorded with incident photon energy of 3500 eV and 5400 eV from the 4-uc sample. (b) Valence band spectra close to Fermi level recorded with incident photon energy of 3500 eV and 5400 eV from the 4-uc sample. The peak around 0.4 eV and 1.2 eV binding energies are known as a coherent and high-energy feature. (c) Background-corrected Fermi level spectra of the 4-uc sample are shown. (d) Background-corrected Fermi level spectra of the 6-uc sample obtained at different photon energies between 3500 eV and 5200 eV. The BE is referenced to the Fermi energy, set at zero, in all panels.

with those reported as coherent and high-energy spectral features in a lightly electron-doped $SrTiO_{3-\delta}$ bulk system [22,26] using ultra-violet photoelectron spectroscopy.

In order to understand the nature and origin of the spectral features, we first note that the spread of the spectral feature being approximately 2 eV, as shown with good statistics for the 4-uc sample in fig. 2(c), is inconsistent with what may be expected on the basis of merely populating the Ti 3*d* states with doped electrons. Taking the well-known density of states of Ti 3*d* in $SrTiO_3$, for example as reported in ref. [25] and populating it with 0.3 e/uc, we estimate the spectral range in this uncorrelated description including the resolution broadening to be $\sim$ 1 eV. Thus, the contrasting experimentally observed spread of $\sim$ 2 eV is clearly indicative of the existence of an additional high-energy feature discussed above. A lineshape analysis, presented in the supplementary material `Supplementarymaterial.pdf` (SM), suggests this high-energy spectral feature to be centered around 1.1 eV BE with a substantial spectral weight ($\sim$ 40% of the total intensity). Such features in the valence band of early transition metal oxides have often been interpreted as the spectroscopic signature of the lower Hubbard band, arising from the Coulomb interaction between electrons within the transition metal 3*d* manifold [22,39,40]. Alternatively, it has also been attributed to oxygen vacancy-induced states specifically in the case of electron doping of $SrTiO_{3-\delta}$ due to the presence of oxygen

vacancies [25,26,28,32] or from electron-phonon interaction [41]. In order to understand whether the Coulomb correlation may indeed account for the observed experimental spectral features, we carried out electronic structure calculations within the combined screened exchange dynamical mean-field theory for lightly doped $SrTiO_3$. We simulate the doping by imposing a specific electron concentration, in the absence of explicit oxygen vacancies. Results of two occupancies of the $3d$ level, namely 0.3 e/uc and 0.035 e/uc in close correspondence to the charge carrier densities at the interface and through the bulk, respectively, are shown in fig. 3(a). The figure makes it clear that there is no spectral intensity in the occupied part for energies below about -0.5 eV for the case of 0.3 e/uc to suggest the existence of a high-binding-energy feature in the photoemission signal; the spectral extension is even less in the case of 0.035 e/uc for the obvious reason of a lower doping of electrons. In order to compare with the experimental data directly, we have multiplied the Ti $3d$ density of states for the 0.3 e/uc case in view of its larger extension into the higher-binding-energy side, shown in fig. 3(a), by the Fermi-Dirac distribution and broadened it with the experimental resolution function. The resulting calculated spectral feature of 0.3 e/uc doped $SrTiO_3$ influenced weakly by the Coulomb interactions is shown in fig. 3(b); for a direct comparison, we also show the low-energy spectral features of the 4-uc sample obtained with 3500 eV photon energy. Clearly, the calculated spectral features are inconsistent with the experimentally observed ones. Specifically, the calculated spectral width is much narrower than in the experiment. We note that the calculated spectral weight of the incoherent part is extremely small at such low doping levels, for example, being 8 and 1% of the total spectral intensity at Ti $3d$ doping levels of 0.3 e/uc and 0.035 e/uc, respectively. This is clearly inconsistent with the experimentally observed spectral weight of $\sim$ 40% in the high-energy feature and, therefore, the feature in the experimental spectra cannot be interpreted as a lower Hubbard band arising from Coulomb correlation effects. It is tempting to interpret the high-energy feature as a plasmon replica of the t_{2g} density of states, in particular since the plasmon energy seen in optical measurements of lightly doped $SrTiO_3$ matches with the energy scale needed ($\omega_p \sim 0.9$ eV). Plasmon contributions to similar high-energy features have recently raised a lot of interest in a related $SrVO_3$ system [42–44]. If a plasmonic replica is present for the low-energy spectral feature of the t_{2g} band, similar replicas will accompany each and every spectral feature from the system with similar relative intensity and energy separation with respect to the primary peak. Thus, we can test the hypothesis of a plasmonic process being responsible to contribute a feature with $\sim$ 40% relative intensity and 1 eV energy separation by carefully analysing any core level spectral feature from the same sample for an evidence of existence of such plasmonic replica. We have carefully analysed the core level Sr $3d$ spectra, presented in fig. S3 of the SM, since it provides one of the sharpest

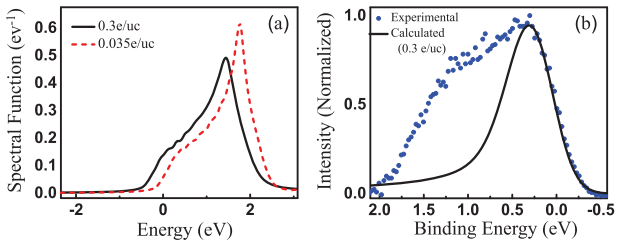

Fig. 3: (Color online)Spectral function of lightly doped $SrTiO_3$ calculated within screened exchange dynamical mean-field theory [45], using the same techniques as described in [42]. (a) Calculated spectral functions for doping levels 0.3 e/uc and 0.035 e/uc are given in terms of number of spin-orbital states per eV and the integrated area over all frequencies under each plot is unity. (b) Spectral functions as in (a) is multiplied by the Fermi function at $T = 300$ K and convoluted with a Gaussian of FWHM 500 meV. The convoluted spectra is normalized at the peak height (multiplied by $\sim$ 6) and is plotted (black solid line) along with the experimental spectra (blue symbols). The energy axis of the calculated spectra is adjusted to plot along with the experimental spectra.

spectral features from this sample. This analysis suggests that the maximum contribution from the plasmonic effect in Sr $3d$ core level spectra can only be $\leq$ 10%. This is incompatible with the experimentally observed spectral weight of $\sim$ 40% in the high-energy feature and, therefore, excludes the possibility of plasmonic effects as the origin of the high-energy feature.

An alternative mechanism for the appearance of a high-energy spectral feature was proposed in ref. [25] in terms of in-gap localized states arising from oxygen vacancies. It is known from charge carrier measurements in oxygen vacancy doped $SrTiO_{3-\delta}$ that the number of free carriers is in general considerably less than what should be anticipated from the vacancy concentration [46]; also high mobility of oxygen vacancies and the tendency of oxygen vacancies in $SrTiO_{3-\delta}$ to cluster are already known in the literature [28,47–50]. In fact, it has even been suggested that the metal-insulator transition and the superconductivity observed in bulk $SrTiO_{3-\delta}$ in the low-δ regime [51] are related to filamentary clustering of oxygen vacancies. [47–49] It is already known that a low level of oxygen vacancies is present in LAO-STO heterostructures [8]. It is also interesting to note that the superconductivity transition temperature observed in LAO-STO heterostructures [3] is close to that observed in the case of bulk $SrTiO_{3-\delta}$. [51] This makes it tempting to attribute the sizable spectral intensity in the high-energy feature to the localizing potential arising from oxygen vacancies in these samples much in the same way as observed for bulk $SrTiO_{3-\delta}$. It is interesting to note in this context that carrying out a detailed resonant photoemission study simultaneously with a novel way to dose different levels of oxygen into the sample, it has been recently shown [32] that a spectral feature at 1.3 eV BE, the weight of which

is correlated with the dose of radiation, can be clearly observed. This indicates that this feature, made visible by the strong resonant enhancement of the relevant cross-section, arises from the presence of oxygen vacancies. A similar high-energy peak has also been observed in photoemission measurements on a pure STO surface [52,53]. The peak position (1.3 eV) observed for this vacancy potential induced in-gap states is consistent with what we observe for the feature designated as high energy in fig. 2(b) (also see fig. S1 in the SM). Thus, our results away from any resonance, in conjunction with results presented in refs. [25,26,28,32] help to establish that as much as $\sim 40\%$, nearly half of the, spectral intensity in our samples stems from the localized in-gap states due to oxygen vacancy potentials.

As mentioned above, in an earlier publication [8], it was established that two distinct types of electron-doped states exist in spatially separated regimes in these samples. Since the dopant sites and doped sites are physically separated by the thickness of the LAO overlayer (~ 3 nm) for the first type, while the dopant and the doped carriers are uniformly spread through the STO layer without any spatial separation for the second type of carriers, it is possible that the electronic structure, namely relative contributions of high-energy and coherent features, corresponding to these two types of doped carriers are different. Unfortunately, the extremely low intensity in photoemission spectrum of these doped carriers does not allow a clear separation of the spectral shapes of the two types of charge carriers. However noting the importance of this aspect, we try to estimate limits on the relative contribution of the high-energy feature to the total spectrum for each type of charge carriers, as follows. First, from the knowledge of the mean free path for inelastic scattering of valence band photoelectrons at 5400 eV photon energies [37] (~ 7.6 nm) and with the width of the 2DEG found for this sample (see ref. [8]), we estimate that $\sim 50\%$ of the total spectral weight in fig. 2(c) is contributed by the 2DEG at a photon energy of 5400 eV. We assume that the 2DEG, being well separated from the oxygen vacancies, contributes only the coherent feature in the valence band spectrum, in order to understand the consequence of this extreme or limiting assumption. This allows us to extract the valence band features of the 3D doped carriers along with the 2DEG doped carriers by subtracting a 50% weight of the total spectrum in terms of a coherent feature only, shown in fig. 4(a). Clearly, the above assumption naturally leads to a spectral feature for the 3D doped part dominated by the in-gap vacancy induced states, peaking at ~ 1.2 eV, shown by the open circles in fig. 4(a). With thus obtained spectral shapes of 2DEG and 3D doped carriers, we further simulate the expected valence band spectra with 3500 eV photon energy, where an estimated smaller mean free path (~ 5.5 nm) leads to $\sim 57\%$ contribution from the 2DEG. The simulated and experimental spectra obtained at 3500 eV photon energy are shown in fig. 4(b). It can be seen from fig. 4(b) that the

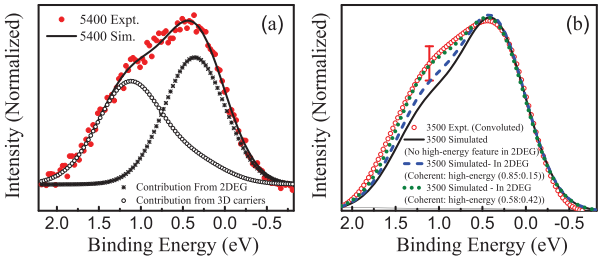

Fig. 4: (Color online) (a) The experimental valence band spectra (red solid dots) obtained with 5400 eV photon energy was simulated (black solid line) with the spectral shapes of the 2DEG (stars) and 3D doped carriers (open symbols). The spectral shape of 2DEG was assumed to have only the coherent spectral feature. (b) The experimental valence band spectrum collected with 3500 eV photon energy (red open symbols) was simulated (black line) with the help of spectral shapes of 2DEG and 3D carriers obtained from the analysis shown in (a). The mismatch is clearly visible. The experimental valence band spectrum of 3500 eV photon energy was convoluted with a Gaussian of ~ 500 meV to have the same effective resolution as of 5400 eV spectrum. The blue dashed line and green dotted line represent similar simulations with coherent : high-energy feature in the 2DEG as (0.85 : 0.15) and (0.58 : 0.42), respectively. The error bar represents the typical error in the experimental data.

high-energy part of the simulated valance band has clearly lower intensity compared to the experimental spectrum obtained at 3500 eV. This suggests that our assumption of 2DEG having only the coherent spectral feature is inconsistent with the experimental valence band spectra and the 2DEG must also contribute in the high-energy region of the valance band. While the uncertainties in the experimental data restrict us to estimate the exact contribution of the 2DEG in the high-energy region, we find that from a minimum ratio of 0.85 : 0.15 up to a maximum ratio of 0.58 : 0.42 between the coherent and high-energy feature is consistent with the experimental spectra within the experimental uncertainties. The result of such simulations are shown as a blue dashed line and a green dotted line in fig. 4(b), respectively.

The above discussion makes it clear that spectral features of both 2DEG at the interface and the bulk-doped charge carriers in the STO crystal are characterized by substantial high-energy intensities that are not captured by detailed theoretical calculations that take into account the correlation effects within the Ti $3d$ manifold of the periodic STO lattice, but it does not account for any effect that breaks this periodicity, for example the presence of oxygen vacancies. The case of the bulk-doped part is somewhat easier to understand based on the past literature, where such high-energy features in oxygen-deficient STO have been attributed to the localizing effects of the vacancy potentials. Since the bulk-doped charge carriers in our system also correspond to the number of vacancies present in the same region of space, it is expected that the vacancy potential will have similar effects on the spectral

signature, allowing us to attribute the high-energy feature seen here in the LAO-STO system to the localized bulk-doped states due to the vacancy potentials. However, the case of the high-energy spectral feature for the interface states needs to be considered differently, since the oxygen vacancies responsible for doping the interface region are found to be present on the top LAO layer [8], thereby being spatially separated from the region where the donated electrons reside. Therefore, any localizing potential from the oxygen vacancies will be negligible for the doped electrons at the interface due to the large spatial separation between the two. In view of this, it is intriguing to find a substantial high-energy feature for the interface spectral properties, established here by showing that less than a minimum contribution ($\geq 15\%$) and up to a maximum of 40% from the high-energy features in the interface states is consistent with experimental results. In order to understand this unexpected result, we speculate the possible formation of polarons at the interface by the interaction of the doped carriers with the atomic lattice. In similar electron-doped system, it is known [41] that the formation of polarons and the interaction of photo-holes with the surrounding lattice can give rise to such high-energy features in the spectral function. Further experimental and theoretical investigations are required to establish the origin of this high-energy feature and to find unambiguously out whether a polaronic effect can indeed be the origin of the missing charge carriers in the interface states.

Conclusion. – In conclusion, we have carried out a high-energy photoelectron spectroscopic investigation to understand the nature and origin of the carriers at the interface of LAO-STO heterostructures. The total spectral intensity is found to be contributed roughly equally by the 2DEG residing in a narrow space region near the interface and by the bulk doping of electrons in the STO crystal due to uniformly distributed oxygen vacancies. Our study shows that 1) experimental valence band spectra near Fermi energy obtained from 4-uc and 6-uc samples clearly contain a low-energy band-like feature and a high-energy localized feature. 2) Theoretical results indicate that the carriers in these dilute doping limits are only weakly correlated and cannot possibly give rise to any prominent signature of the lower Hubbard band at higher energies. 3) Considering the spectrum of the bulk-doped STO crystal, the prominent high-energy feature with a peak at $\sim 1.2\,\mathrm{eV}$ is attributed to the localizing potentials of oxygen vacancies within $SrTiO_3$. 4) Our results show that the spectral features associated with the 2DEG interface states also have a substantial high-energy feature, though the origin of this feature cannot be associated with the oxygen vacancy potential due to a spatial separation of the doped electrons and the corresponding oxygen vacancy locations. Thus, we suggest that polaronic effects may be responsible in giving rise to the high-energy feature in the case of the 2DEG at the interface. 5) The observation of such localized states, independent of their origin, within the 2DEG and 3D doped carrier suggests substantial reductions of carriers available for transport in the respective regions.

* * *

We thank the Department of Science and Technology, Government of India for financial support. Our work was further supported by IDRIS/GENCI Orsay under project t2017091393, and the European Research Council under its Consolidator Grant scheme (project 617196). DDS thanks Jamsetji Tata Trust for support.

REFERENCES

[1] Ohtomo A. and Hwang H. Y., *Nature*, **427** (2004) 423.
[2] Thiel S., Hammerl G., Schmehl A., Schneider C. W. and Mannhart J., *Science*, **313** (2006) 1942.
[3] Reyren N., Thiel S., Caviglia A. D., Kourkoutis L. F., Hammerl G., Richter C., Schneider C. W., Kopp T., Rüetschi A.-S., Jaccard D., Gabay M., Muller D. A., Triscone J.-M. and Mannhart J., *Science*, **317** (2007) 1196.
[4] Caviglia A. D., Gariglio S., Reyren N., Jaccard D., Schneider T., Gabay M., Thiel S., Hammerl G., Mannhart J. and Triscone J. M., *Nature*, **456** (2008) 624.
[5] Bert J. A., Kalisky B., Bell C., Kim M., Hikita Y., Hwang H. Y. and Moler K. A., *Nat. Phys.*, **7** (2011) 767.
[6] Dikin D. A., Mehta M., Bark C. W., Folkman C. M., Eom C. B. and Chandrasekhar V., *Phys. Rev. Lett.*, **107** (2011) 056802.
[7] Brinkman A., Huijben M., van Zalk M., Huijben J., Zeitler U., Maan J. C., van der Wiel W. G., Rijnders G., Blank D. H. A. and Hilgenkamp H., *Nat. Mater.*, **6** (2007) 493.
[8] Mukherjee S., Pal B., Choudhury D., Sarkar I., Drube W., Gorgoi M., Karis O., Takagi H., Matsuno J. and Sarma D. D., *Phys. Rev. B*, **93** (2016) 245124.
[9] Sing M., Berner G., Goss K., Müller A., Ruff A., Wetscherek A., Thiel S., Mannhart J., Pauli S. A., Schneider C. W., Willmott P. R., Gorgoi M., Schäfers F. and Claessen R., *Phys. Rev. Lett.*, **102** (2009) 176805.
[10] Cancellieri C., Reinle-Schmitt M. L., Kobayashi M., Strocov V. N., Schmitt T., Willmott P. R., Gariglio S. and Triscone J.-M., *Phys. Rev. Lett.*, **110** (2013) 137601.
[11] Berner G., Sing M., Fujiwara H., Yasui A., Saitoh Y., Yamasaki A., Nishitani Y., Sekiyama A., Pavlenko N., Kopp T., Richter C., Mannhart J., Suga S. and Claessen R., *Phys. Rev. Lett.*, **110** (2013) 247601.
[12] Drera G., Banfi F., Federici Canova F., Borghetti P., Sangaletti L., Bondino F., Magnano E., Huijben J., Huijben M., Rijnders G., Blank D. H. A., Hilgenkamp H. and Brinkman A., *Appl. Phys. Lett.*, **98** (2011) 052907.

[13] Popović Z. S., Satpathy S. and Martin R. M., *Phys. Rev. Lett.*, **101** (2008) 256801.

[14] Delugas P., Filippetti A., Fiorentini V., Bilc D. I., Fontaine D. and Ghosez P., *Phys. Rev. Lett.*, **106** (2011) 166807.

[15] Nakagawa N., Hwang H. Y. and Muller D. A., *Nat. Mater.*, **5** (2006) 204.

[16] Willmott P. R., Pauli S. A., Herger R., Schlepütz C. M., Martoccia D., Patterson B. D., Delley B., Clarke R., Kumah D., Cionca C. and Yacoby Y., *Phys. Rev. Lett.*, **99** (2007) 155502.

[17] Bristowe N. C., Littlewood P. B. and Artacho E., *Phys. Rev. B*, **83** (2011) 205405.

[18] Siemons W., Koster G., Yamamoto H., Harrison W. A., Lucovsky G., Geballe T. H., Blank D. H. A. and Beasley M. R., *Phys. Rev. Lett.*, **98** (2007) 196802.

[19] Herranz G., Basletić M., Bibes M., Carrétéro C., Tafra E., Jacquet E., Bouzehouane K., Deranlot C., Hamzić A., Broto J.-M., Barthélémy A. and Fert A., *Phys. Rev. Lett.*, **98** (2007) 216803.

[20] Liu Z. Q., Li C. J., Lü W. M., Huang X. H., Huang Z., Zeng S. W., Qiu X. P., Huang L. S., Annadi A., Chen J. S., Coey J. M. D., Venkatesan T. and Ariando, *Phys. Rev. X*, **3** (2013) 021010.

[21] Li Y., Phattalung S. N., Limpijumnong S., Kim J. and Yu J., *Phys. Rev. B*, **84** (2011) 245307.

[22] Sarma D. D., Barman S. R., Kajueter H. and Kotliar G., *EPL (Europhysics Letters)*, **36** (1996) 307.

[23] Sarma D. D., Barman S. R., Kajueter H. and Kotliar G., *Phys. B: Condens. Matter*, **223-224** (1996) 496.

[24] Fujimori A., Hase I., Nakamura M., Namatame H., Fujishima Y., Tokura Y., Abbate M., de Groot F. M. F., Czyzyk M. T., Fuggle J. C., Strebel O., Lopez F., Domke M. and Kaindl G., *Phys. Rev. B*, **46** (1992) 9841.

[25] Shanthi N. and Sarma D. D., *Phys. Rev. B*, **57** (1998) 2153.

[26] Aiura Y., Hase I., Bando H., Yasue T., Saitoh T. and Dessau D. S., *Surf. Sci.*, **515** (2002) 61.

[27] Hüfner S., *Z. Phys. B: Condens. Matter*, **61** (1985) 135.

[28] Jeschke H. O., Shen J. and Valent R., *New J. Phys.*, **17** (2015) 023034.

[29] Siemons W., Koster G., Yamamoto H., Geballe T. H., Blank D. H. A. and Beasley M. R., *Phys. Rev. B*, **76** (2007) 155111.

[30] Koitzsch A., Ocker J., Knupfer M., Dekker M. C., Dörr K., Büchner B. and Hoffmann P., *Phys. Rev. B*, **84** (2011) 245121.

[31] Sing M., Jeschke H. O., Lechermann F., Valentí R. and Claessen R., *Eur. Phys. J. ST*, **226** (2017) 2457.

[32] Gabel J., Zapf M., Scheiderer P., Schütz P., Dudy L., Stübinger M., Schlueter C., Lee T.-L., Sing M. and Claessen R., *Phys. Rev. B*, **95** (2017) 195109.

[33] Fadley C. S. and Nemk S., *J. Electron Spectrosc. Relat. Phenom.*, **195** (2014) 409.

[34] Mukherjee S., Knut R., Mohseni S. M., Anh Nguyen T. N., Chung S., Tuan Le Q., Åkerman J., Persson J., Sahoo A., Hazarika A., Pal B., Thiess S., Gorgoi M., Anil Kumar P. S., Drube W., Karis O. and Sarma D. D., *Phys. Rev. B*, **91** (2015) 085311.

[35] Kozina X., Ouardi S., Balke B., Stryganyuk G., Fecher G. H., Felser C., Ikeda S., Ohno H. and Ikenaga E., *Appl. Phys. Lett.*, **96** (2010) 072105.

[36] Claessen R., Sing M., Paul M., Berner G., Wetscherek A., Müller A. and Drube W., *New J. Phys.*, **11** (2009) 125007.

[37] Pal B., Mukherjee S. and Sarma D., *J. Electron Spectrosc. Relat. Phenom.*, **200** (2015) 332.

[38] Thiess S., Lee T. L., Bottin F. and Zegenhagen J., *Solid State Commun.*, **150** (2010) 553.

[39] Imada M., Fujimori A. and Tokura Y., *Rev. Mod. Phys.*, **70** (1998) 1039.

[40] Georges A., Kotliar G., Krauth W. and Rozenberg M. J., *Rev. Mod. Phys.*, **68** (1996) 13.

[41] Fujimori A., Bocquet A., Morikawa K., Kobayashi K., Saitoh T., Tokura Y., Hase I. and Onoda M., *J. Phys. Chem. Solids*, **57** (1996) 1379.

[42] van Roekeghem A. and Biermann S., *EPL*, **108** (2014) 57003.

[43] Tomczak J. M., Casula M., Miyake T., Aryasetiawan F. and Biermann S., *EPL*, **100** (2012) 67001.

[44] Boehnke L., Nilsson F., Aryasetiawan F. and Werner P., *Phys. Rev. B*, **94** (2016) 201106.

[45] van Roekeghem A., Ayral T., Tomczak J. M., Casula M., Xu N., Ding H., Ferrero M., Parcollet O., Jiang H. and Biermann S., *Phys. Rev. Lett.*, **113** (2014) 266403.

[46] Gong W., Yun H., Ning Y. B., Greedan J. E., Datars W. R. and Stager C. V., *J. Solid State Chem.*, **90** (1991) 320.

[47] Cordero F., *Phys. Rev. B*, **76** (2007) 172106.

[48] Szot K., Speier W., Carius R., Zastrow U. and Beyer W., *Phys. Rev. Lett.*, **88** (2002) 075508.

[49] Szot K., Speier W., Bihlmayer G. and Waser R., *Nat. Mater.*, **5** (2004) 312.

[50] Cuong D. D., Lee B., Choi K. M., Ahn H. S., Han S. and Lee J., *Phys. Rev. Lett.*, **98** (2007) 115503.

[51] Schooley J. F., Hosler W. R. and Cohen M. L., *Phys. Rev. Lett.*, **12** (1964) 474.

[52] Santander-Syro A. F., Copie O., Kondo T., Fortuna F., Pailhs S., Weht R., Qiu X. G., Bertran F., Nicolaou A., Taleb-Ibrahimi A., Le Fvre P., Herranz G., Bibes M., Reyren N., Apertet Y., Lecoeur P., Barthlmy A. and Rozenberg M. J., *Nature*, **469** (2011) 189.

[53] Meevasana W., King P. D. C., He R. H., Mo S.-K., Hashimoto M., Tamai A., Songsiriritthigul P., Baumberger F. and Shen Z.-X., *Nat. Mater.*, **10** (2011) 114.